NJC

New Journal of Chemistry

A journal for new directions in chemistry

Accepted Manuscript

This article can be cited before page numbers have been issued, to do this please use: I. K. Attatsi, W. Zhu and X. Liang, *New J. Chem.*, 2020, DOI: 10.1039/C9NJ02408E.

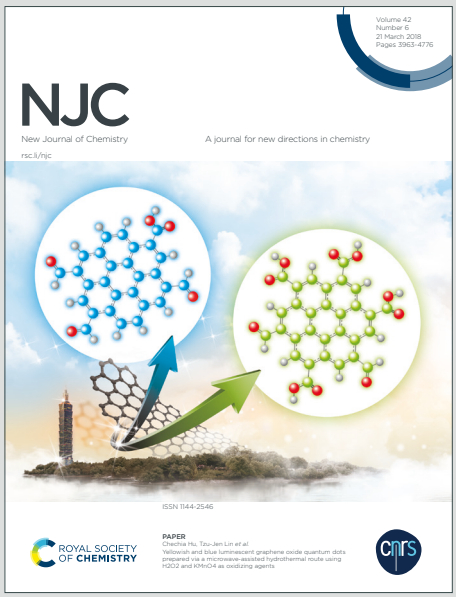

This is an Accepted Manuscript, which has been through the Royal Society of Chemistry peer review process and has been accepted for publication.

Accepted Manuscripts are published online shortly after acceptance, before technical editing, formatting and proof reading. Using this free service, authors can make their results available to the community, in citable form, before we publish the edited article. We will replace this Accepted Manuscript with the edited and formatted Advance Article as soon as it is available.

You can find more information about Accepted Manuscripts in the Information for Authors.

Please note that technical editing may introduce minor changes to the text and/or graphics, which may alter content. The journal's standard Terms & Conditions and the Ethical guidelines still apply. In no event shall the Royal Society of Chemistry be held responsible for any errors or omissions in this Accepted Manuscript or any consequences arising from the use of any information it contains.

View Article Online
DOI: 10.1039/C9NJ02408E

ARTICLE

Noncovalent Immobilization of Co(II)porphyrin through Axial Coordination as an Enhanced Electrocatalyst on Carbon Electrode for Oxygen Reductions and Evolutions

Received 00th January 20xx,
Accepted 00th January 20xx

DOI: 10.1039/x0xx00000x

Isaac Kwaku Attatsi[a], Weihua Zhu[a,b]* and Xu Liang[a,b]*

Catalysis of fuel-producing reactions can be transferred from homogeneous solution to surface via attachment of the molecular catalyst. A pyrene-pyridine hybrid (Py-Py) was used as an axial ligand to bridge Co(II)tetraphenylporphyrin which was finally immobilized on carbon nanotubes via noncovalent interactions and further deposited on glassy carbon. This noncovalent immobilization of Co(II)porphyrin through axial coordination provides significantly enhanced electrochemically catalyzed oxygen reductions and oxygen evolutions, illustrating a new insight into understanding surface catalysis.

Introduction

The ever-growing demands for fossil fuels accompanied by increasing environmental pollutions emanating from fossil depletion has been a matter of concern to researchers [1–3]. This resulted to an extensive search for a new renewable energy source that is clean, cheap and efficient with zero emission. Technological advancement into energy production led to development of fuel cells such as metal-air batteries [4–7], microbial fuel cells [8,9], direct solar driven water splitting [10–14] and other forms of regenerative fuel cells. Oxygen reduction and evolution (ORR and OER) play an important role in these various renewable energy conversion systems. To this extent the designing and development of catalysts for ORR and OER are at the heart of researchers towards the advancement of renewable energies. Traditionally, Pt based catalysts and oxides of other noble metals of Iridium and ruthenium are employed in ORR and OER respectively [15] but are limited due to low natural abundance and high cost. Methanol poisoning arising from Pt based catalyst is another ground to look for safer and highly desirable catalyst for ORR and OER. The development of low cost and earth abundant 3d transition metals of Co, Ni, Mn and Fe catalysts offer a promising route to compete with platinum barometer [16–20]. Metalloporphyrins with their high catalytic properties are increasingly being modified and rationally designed to effectively serve as a means of reducing or evolving oxygen [21–23] in fuel cells. Zhang and co-workers reported cobalt porphyrins functionalized on carbon support is effective for ORR [24]. Mao and co-workers reported an efficient electrocatalyst for ORR derived from a cobalt porphyrin-based covalent organic framework [25]. Sonkar and co-workers also synthesized different kinds of substituted cobalt porphyrins and compared their ORR activities to simple cobalt porphyrin [15]. Maurin and Robert did noncovalent immobilization of a molecular metalloporphyrin electrocatalyst using carbon electrodes towards CO_2 conversion [26]. From their work a pyrene-appended iron porphyrin bearing OH groups on phenyl rings was immobilized on carbon nanotubes via noncovalent interactions. Their work showed enhanced catalytic performance. Based on these previous works, we selected a medium that is most appropriate to further enhance the electrocatalytic behaviour when coordinated to the metal centre of porphyrin with stability of the system in mind. This led to synthesis of **1** and Py-Py compound which when axially bonded could effectively improve the catalytic performance of our system on MWCNT support. In other to investigate this, we herein report a new strategy to construct metallopophyrin@MWCNTs nanocomposite with pyrene-pyridine hybrid (Py-Py) used as an axial ligand to bridge Co(II)tetraphenylporphyrin which was finally immobilized on carbon nanotubes via noncovalent interactions and further deposited on glassy carbon. Comparatively, the enhanced electrocatalytic behaviour shown by **1**/MWCNT/Py-Py is as a result of the axial ligand system (Py-Py) coordinated to Co(II)tetraphenylporphyrin. This means rationally tuning the electrocatalytic environment instead of the active catalytic center is a promising strategy to improve ORR and OER.

Experimental

Functionalization of MWCNTs

[a] *School of Chemistry and Chemical Engineering, Jiangsu University, Zhenjiang 212013, P. R. China. E-mail: liangxu@ujs.edu.cn, Tel@Fax: +86-511-8879-1928 (to X. L.); E-mail: sayman@ujs.edu.cn, Tel@Fax: +86-511-8879-1928 (to W. Z.)*
[b] *State Key Laboratory of Coordination Chemistry, Nanjing University, Nanjing 210000, P. R. China*
† Footnotes relating to the title and/or authors should appear here.
Electronic Supplementary Information (ESI) available: [details of any supplementary information available should be included here]. See DOI: 10.1039/x0xx00000x

View Article Online
DOI: 10.1039/C9NJ02408E

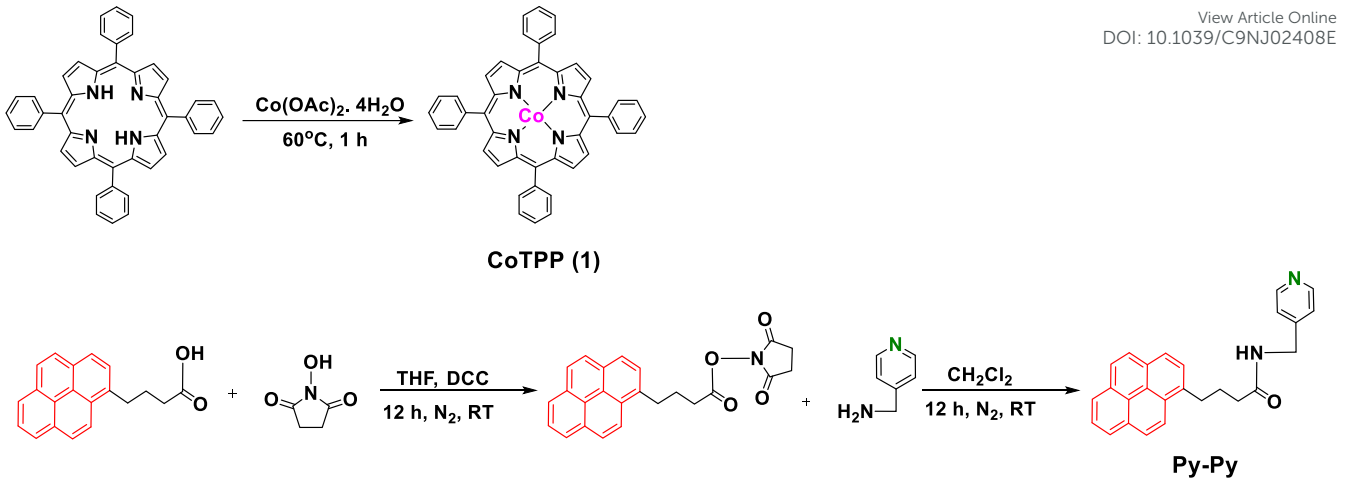

Scheme 1. Synthesis of Co(II)porphyrin (**1)** and pyrene-pyridine hybrid (**Py-Py**).

A known mass of 2.0 mM Py-Py was mixed with 5.0 mg MWCNT and sonicated for 30 min in 5 mL isopropyl alcohol (IPA) nafion mixture. The mixture was stirred for 24 h, filtered and washed. It was dried under vacuum for 24 h and labelled MWCNT/Py-Py composite. 1mg of the composite was measured and mixed with 1 mL IPA and sonicated for 30 min. After 1.0 mM co(II)porphyrin was added to the surfaced modified MWCNTs IPA solution and the mixture stirred for 12 h at room temperature. This composite material was filtered, washed with 5 mL IPA (to remove any weakly adsorbed Co(II)porphyrin), dried under vacuum and labelled as **1/MWCNT/Py-Py.** The unfunctionalized MWCNTs (1.0 mg) were also mixed with Co(II)porphyrin (1.0 mM) at same reaction conditions and process to give **1/MWCNT**. The prepared materials (**1/MWCNT/Py-Py** and **1/MWCNT**) were used for SEM, XRD, UV, FT-IR and EPR characterizations.

Electrode Modification

A 2 µL suspension of the composite (MWCNT/Py-Py) was drop coated on surface of glass carbon electrode (GC) thrice and allowed to dry for 2 h. Prior to drop coating of composite onto GC, the surface was polished with 0.05 µm alumina and rinsed with doubly distilled water in ultrasonic bath to remove any adhered Al_2O_3 particles. It was rinsed with ethanol and dried under room temperature for about 10 min. The modified GC electrode (GC/MWCNT/Py-Py) was immersed in a 1.0 mM CH_2Cl_2 solution of **1** (Co(II)porphyrin) and stored for 12 h to achieve coordination to the metal centre of the porphyrin. The modified electrode was removed from the Co(II)porphyrin solution, dried and washed with 5 mL CH_2Cl_2 until almost colourless solution was observed. The washing was to purposely remove any weakly adsorbed Co(II)porphyrin [27–31]. It was air dried for 1-2 h, labelled as **1/MWCNT/Py-Py** and ready for ORR and OER experiments. Steps and processes to obtain GC/MWCNT with immobilized Co(II)porphyrin (**1/MWCNT**) is similar to **1/MWCNT/Py-Py** with difference in absence of Py-Py moiety.

Results and discussion

Structural Characterization

The morphology of MWCNT, **1/MWCNT,** MWCNT/Py-Py and **1/MWCNT/Py-Py** composites were confirmed by using scanning electron microscopy. As shown in **Figure 1,** the nanotubes appeared visibly clear with a uniform capsule-like morphology. Nodular topography with less or no aggregation as seen in **Figure 1** illustrates uniform distribution of **1** on the surface of the MWCNT [31,32]. This appearance was similar in **1/**MWCNT**,** MWCNT/Py-Py and **1/MWCNT/Py-Py** composites. As shown in **Figure 2a**, powder x-ray diffraction (XRD) patterns of MWCNT showed two diffraction signals at 2θ = 25.8° and 43.3° which corresponds to MWCNT structure [33,34]. Characteristic features of **1** were exhibited at 2θ = 25.8° and 45.0° (weak) in **1/MWCNT** and **1/MWCNT/Py-Py** which is in line with metalloporphyrin XRD patterns. Composite materials of **1/MWCNT** and **1/MWCNT/Py-Py** maintained a strong diffraction signal at 2θ = 25.8° which illustrates the graphitic nature of MWCNT is retained [35]. The appearance of characteristic peaks at 45.0° (111) indicates the Co(II)porphyrin is completely encapsulated within the graphitic carbon [36]. It is worthy to note that weak diffraction feature of cobalt could occur, and this is when the mass of **1** in the composites is low or the temperature applied to composite before characterization is not strong enough [37]. UV-vis spectra of **1** revealed an intense Soret band peak at λ = 409 nm whereas Q band absorptions appeared at λ = 526 nm (**Fig. 2b**). Coordination interactions between **1** and Py-Py, were firstly investigated in CH_2Cl_2 devoid of carbon nanotubes as shown in **Fig. S4.** The Co(II)porphyrin peaks were retained at 409 nm and 526 nm with emergence of Py-Py peak between 300-350 nm indicating a week interaction. Also noted is a weak peak at 433 nm which might be the source of **1** and Py-Py coordination. In other to understand this interaction further, we compared the UV-Vis absorption spectra of **1**/Py-Py to that of **1** and pure pyridine mixture. As shown in the spectra, addition of microliters of pyridine introduces peaks at 433 nm same as that of **1**/Py-Py.

View Article Online
DOI: 10.1039/C9NJ02408E

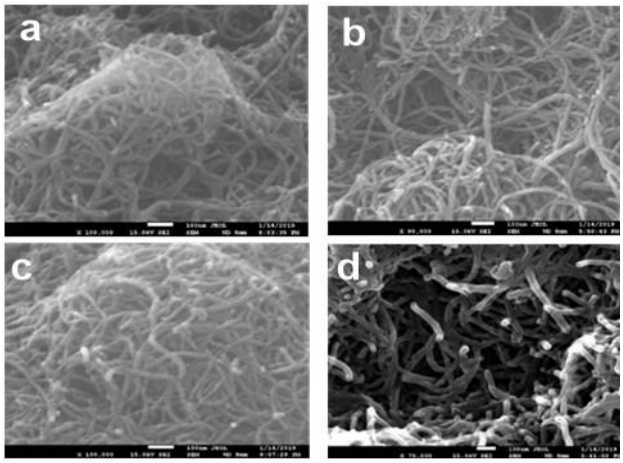

Figure 1. SEM images of MWCNT (a), **1**/MWCNT (b), MWCNT/Py-Py (c) and **1**/MWCNT/Py-Py (d) materials.

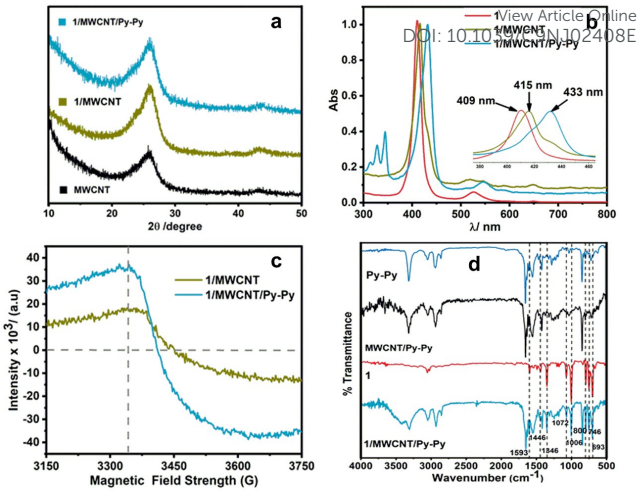

Figure 2. XRD patterns (a), UV-Vis absorption spectra in CH_2Cl_2 (b), EPR (c), and FT-IR (d) of composites.

This therefore is a clear evidence the metal center of 1 coordinated through the pyridine of our Py-Py, on its axial positions. Composite materials from **1/MWCNT** and **1/MWCNT/Py-Py** were also characterized using UV-Vis spectroscopic technique. Spectra of the **1/MWCNT** showed a slight shift of Soret band to λ = 415 nm. This indicates an interaction between **1** and MWCNTs [28] which also confirmed the presence of metallic cobalt through XRD analysis. In the case of **1/MWCNT/Py-Py** composite, a larger red-shift of the absorptions has been observed in both Soret (433 nm) and Q bands (545 nm) regions indicating an interaction between MWCNT, **1** and Py-Py. It is important to reiterate that the Py-Py linker serves as a coordination ligand responsible for axial coordination to the cobalt centre [38,39]. The appearance of a new soret peak of **1/MWCNT/Py-Py** without appearance of **1/MWCNT** peaks indicates all **1** has been coordinated with Py-Py [40] as shown in the (**Fig. 2b**). Spectra for **1/MWCNT/Py-Py** (**Fig. 2b**) further explains changes in geometrical symmetry and electronic density [41] of **1** upon introduction of Py-Py which is as a result of axial coordination of py-py towards the Co (II) ion of **1** [29,42,43]**.** This was also demonstrated by solid state electron paramagnetic resonance (EPR) spectra of nanocomposites where **1/MWCNT/Py-Py** nanocomposite has revealed a decreased magnetic field strength value compared with **1/MWCNT** that clearly reflected the changes of coordination environment. FTIR spectra of our composite materials are shown in **Fig. 2d** (**1/MWCNT/Py-Py**) and **Fig. S5** (**1/MWCNT**)**.** MWCNT (**Fig. S5,** top) showed a strong and broad band around 3425 cm^{-1} attributed to the presence of -OH or -COOH [29] functional group and a very weak band at 1545 cm^{-1} in the fingerprint region attributed to C=C vibrations. **1/MWCNT** (**Fig. S5,** bottom) composite showed characteristic strong and broad band at 3430 cm^{-1} showing presence of -OH or -COOH [29,44] emanating from MWCNT. A weak band that appeared at 3052 cm^{-1} results from the C-H stretching in phenyl ring of **1** while that of 2931 cm^{-1} represents symmetric and antisymmetric alkyl C-H vibrations of the porphyrin ring [45]. Peaks at 1596 cm^{-1} (C=C stretching vibrations of phenyl rings) [46], 1349 cm^{-1} (C-N), 1076 cm^{-1} (C=C symmetric stretching of pyrrole ring), 1003 cm^{-1} (C-C vibrations of pyrrole ring) [47], 703 cm^{-1} (C-N) and 750 cm^{-1} (C-N out of plane bending)[47] are all characteristic peaks of **1**. The presence of these peaks provides evidence of **1** in the composite mixture (**1/MWCNT**). Spectra from Py-Py, Py-Py/MWCNT, and **1** all appeared in **1/MWCNT/Py-Py** (**Fig. 2d).** The appearance of **1** and Py-Py peaks in this spectrum confirms the formation of the composite [48] an indication that all products have been successfully intercalated. This also further proves the presence of metallic cobalt in our composite materials as indicated with black dotted lines. It is worthy to note that the addition of **1** to Py-Py/MWCNT showed no change in peak positions of **1** indicating there was a little or no change in functional group during adsorption.

Table1: CV comparisons of ORR activities of **1/MWCNT/Py-Py** and **1/MWCNT** in different aqueous solutions.

Catalyst	Aqueous media	Onset potential for ORR (V vs RHE)	Peak potential (V vs RHE)	Current densities ($mA.cm^{-2}$)
1/MWCNT/Py-Py	H_2SO_4	+ 0.584	+ 0.375	10.07
	PBS	+ 0.512	+ 0.253	4.53
	KOH	+ 0.890	+ 0.766	3.732
1/MWCNT	H_2SO_4	+ 0.583	+ 0.203	0.771
	PBS	+ 0.519	+ 0.222	0.939
	KOH	+ 0.880	+ 0.701	0.665

View Article Online
DOI: 10.1039/C9NJ04085E

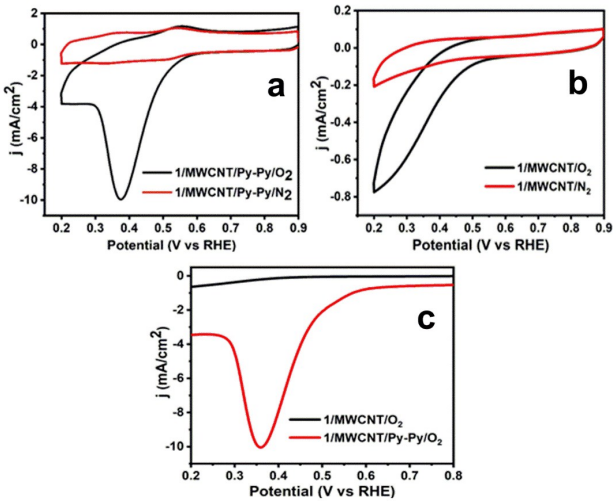

Figure 3. CVs of GC electrodes coated with (a) **1**/MWCNT/Py-Py, (b) **1**/MWCNT and (c) LSV of GC electrodes coated with **1**/MWCNT/Py-Py and **1**/MWCNT under N_2 or O_2 in 0.5 M $H_2SO_{4(aq)}$. Conditions: 50 mV s^{-1} scan rate at 25 °C.

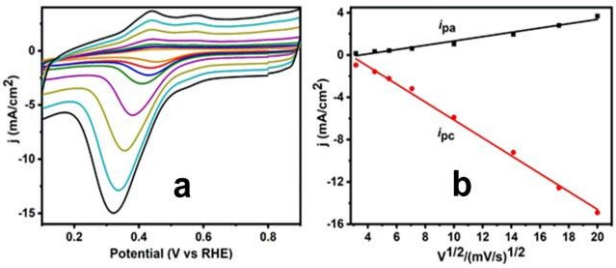

Figure 4. CV response of **1**/MWCNT/Py-Py at different scan rates (a) Plot of anodic and cathodic peak currents *vs* square roots of scan rate (b) in 0.5 M H_2SO_4 solution.

Electrochemically Catalyzed ORRs

Electrochemically catalysed oxygen reduction reaction is an important reaction since it is one of the key determinants for realization of hydrogen-based society. In the current study, cyclic voltammetry (CV) was firstly carried in 0.5 M H_2SO_4 (pH ≈ 0) to examine the ORR catalytic activity of **1** axially linked Py-Py on MWCNT (**1/MWCNT/Py-Py**) support at a scan rate of 50 mV s^{-1} (**Fig. 3a**). Under N_2 atmosphere, the CV curve within the scanned potential ranges presented almost featureless slope for the cathodic current. In a sharp contrast, an explicit positive peak potential of + 0.375 V and a high and stable current density at 10.07 mA.cm^{-2} were observed with an onset at + 0.584 V. Comparisons were made between a direct **1** self-assembled on GC electrode with MWCNT support (**Fig. 3b**) and **1/MWCNT/Py-Py**. We observed that although the onset potentials were similar, there was a great difference by more than 5 times in the current densities. While **1/MWCNT** showed current density at 0.77 mA.cm^{-2}, **1/MWCNT/Py-Py** exhibited an outstanding catalytic peak with current density of 10.07 mA.cm^{-2}. Also, the peak potentials of **1/MWCNT** were observed at E = + 0.203 V which is less positive than **1/MWCNT/Py-Py** whose peak potential was E = + 0.375 V. This similar trend was observed in LSV as shown in **Fig. 3c.** This is an indication of **1/MWCNT/Py-Py** showing high ORR catalytic efficiency as compared to **1/MWCNT**. Sonkar and co-workers also tested ORR in acidic medium for three different kinds of cobalt porphyrins whose observed onset potentials were E = + 0.43, + 0.44 and + 0.49 V for MWCNT/CoTPP, MWCNT/CoTCPP and MWCNT/CoTHPP respectively with lower corresponding current densities [15]. The onset potentials, peak potentials, and current densities presented herein for **1/MWCNT/Py-Py** are by far greater than theirs in acidic medium under similar conditions. Comparison was further extended to commercial 20 wt% platinum–carbon (Pt/C) catalysts which is reported to show an onset at E = + 0.88 V [15] which is more positive than our work. Despite high onset, the limiting current density for the **1/MWCNT/Py-Py** moiety is by far 10.07 mA.cm^{-2} greater as appeared in the CV curve for the Pt/C [15] when the electrolyte was saturated with O_2, suggesting a pronounced catalytic activity for our catalyst towards ORR. This means the **1/MWCNT/Py-Py** materials could serve as an alternative to the expensive Pt/C catalyst under similar conditions. CV data of different scan rates (10–400 mVs^{-1}) at **1/MWCNT/Py-Py** electrode in 0.5 M H_2SO_4 showed increase in anodic and cathodic peak currents (**Fig. 4a**). A plot of the peak current *vs.* square root of scan rate (**Fig. 4b**) shows a linear relationship (R = 0.98) which indicates the electrochemical process is diffusion controlled [49]. Oxygen reduction reaction activities were also monitored in various pH values, such as PBS (pH ≈ 7) and KOH (pH ≈ 14). It was clearly demonstrated the onset potentials of the two materials (**1/MWCNT/Py-Py** and **1/MWCNT**) are similar but there appears a great difference in current densities. **1/MWCNT/Py-Py** pronounced an outstanding catalytic performance toward ORR more than **1/MWCNT** in both solutions as shown in LSV data (**Fig. 5a and 5b**).

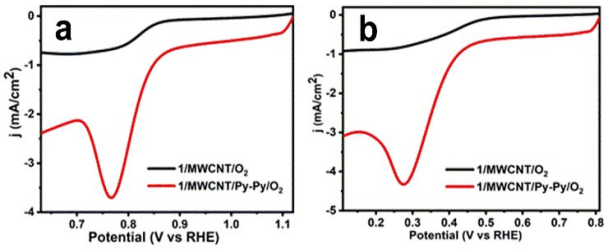

Figure 5. LSV of GC electrodes coated with **1**/MWCNT/Py-Py and **1**/MWCNT under O_2 in (a) 1.0 M KOH and (b) 0.1 M PBS. Conditions: 50 mV s^{-1} scan rate at 25 °C.

CV data (**Fig. S6 and S7**) obtained showed similar result as that of LSV in both aqueous solutions. The onset potentials, peak potentials and current densities are all summarized in **Table 1**. The stability of the materials (**1/MWCNT/Py-Py** and **1/MWCNT**) were investigated in $H_2SO_{4(aq)}$. This was studied when substrates used earlier for CV and LSV experiments in acidic medium were washed with several milliliters of CH_2Cl_2 and LSV experiment run again. They all showed subtle stability in acidic medium as illustrated in **Figure 6**.

View Article Online
DOI: 10.1039/C9NJ04085E

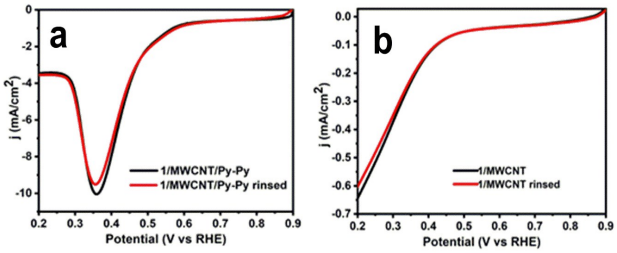

Figure 6. LSVs of GC electrodes coated with (a) **1/MWCNT/Py-Py** and (b) **1/MWCNT** in 0.5 M H_2SO_4 (aq) solution before and after rinsing with 5 mL CH_2Cl_2. Conditions: 50 mV s^{-1} scan rate at 25 °C.

Electrochemically Catalyzed OERs

In other to investigate the OER activity of **1** on MWCNT/Py-Py and MWCNT, CV experiments were carried out in 0.1 M PBS and 1.0 M KOH. In PBS, **1/MWCNT/Py-Py** displayed a very high catalytic current at j = 45 mA.cm^{-2} (E = 2.6 V) with onset at 1.7 V (**Fig. 7a**). **1**/MWCNT with similar onset at 1.7 V displayed its current density at j = 35 mA.cm^{-2}. At j = 10 mA.cm^{-2}, an onset overpotential of 650 mV (**Fig. 7a**) was obtained for **1/MWCNT/Py-Py** while that of **1/MWCNT** was 790 mV (**Fig. 7b**). It is worthy to note that the onset overpotential of **1/MWCNT/Py-Py** is 140 mV less than **1/MWCNT** an indication that OER activity of **1/MWCNT/Py-Py** is best owing to presence of Py-Py.

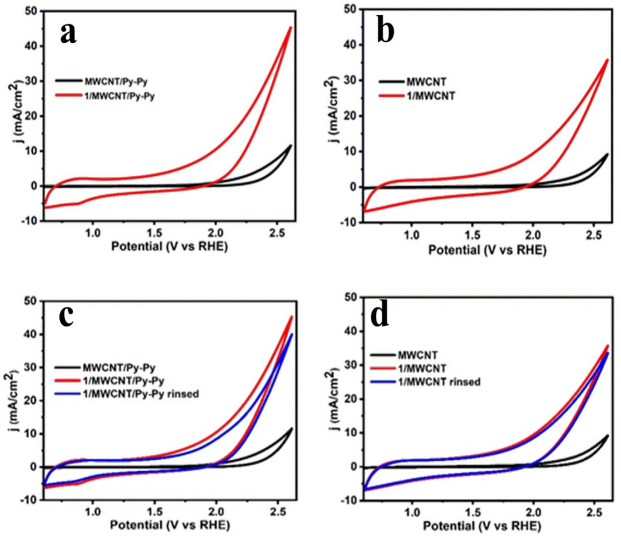

Figure 7. CVs of GC electrodes coated with (a) **1/MWCNT/Py-Py**, (b) **1/MWCNT** in 0.1 M PBS. (c) **1/MWCNT/Py-Py** and (d) **1/MWCNT** in 0.1 M PBS solution before and after rinsing with CH_2Cl_2. Conditions: 50 mV s^{-1} scan rate at 25 °C.

OER activity of our material (**1/MWCNT/Py-Py)** was further compared with the works of Wang and co-workers where cationic cobalt porphyrin was used for OER. They reported OER onset overpotential activity at j = 1.0 mA.cm^{-2} to a little over 400 mV [50]. In our work at j = 1.0 mA.cm^{-2} an onset overpotential of 400 mV was recorded which is quite better than works of Wang and co-workers, another evidence of enhanced activity of **1/MWCNT/Py-Py** compared to **1/MWCNT**. Surface stability of our materials were checked after rinsing with CH_2Cl_2 and subjected to electrocatalytic OER activity. The results as shown in **Fig. 7c** indicates the rinsed **1/MWCNT/Py-Py** lost activity of about 8% while **1/MWCNT** lost activity of about 4% (**Fig. 7d**). LSV **(Fig. 8a)** data obtained in KOH showed a much higher catalytic activity than those exhibited in PBS. In addition, at j = 10 m. Acm^{-2} an onset overpotential of 440 mV was recorded at an onset of 1.67 V for **1/MWCNT/Py-Py** which is smaller than 480 mV recorded for **1/MWCNT** at same j value. Comparing the onset overpotentials for **1/MWCNT/Py-Py** in both PBS and KOH, the latter is highly recommended since OER catalysis is more enhanced.

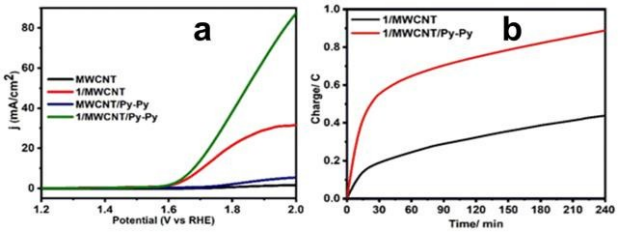

Figure 8. LSVs of GC electrodes coated with (a) MWCNT, **1/MWCNT**, MWCNT/Py-Py and **1/MWCNT/Py-Py** in 1.0 M KOH at 50 mV s^{-1} scan rate (b) Controlled-potential electrolysis at E = +2.25 V (RHE) in 0.1 M PBS using GC electrodes coated with **1**/MWCNT and **1**/MWCNT/Py-Py at 25 °C.

Controlled-bulk electrolysis was performed in 0.1 M PBS using GC as a working electrode coated with **1/MWCNT/Py-Py**, Pt wire as the counter electrode and SCE as reference electrode. The potential was set to E = (+2.25 V, RHE) and experiment run for 240 min (**Fig. 8b**). The amount of O_2 evolved could be seen largely as bubbles on the electrode. That of **1/MWCNT** is far less compared to **1/MWCNT/Py-Py (Fig. 8b)**. Based on the results presented in this work, we conclude that introduction of py-py moiety which served as a linker is responsible for the enhanced electrocatalyzed ORR and OER activities. The pyrene unit in the py-py increased π-π staking interaction on carbon support.

Conclusions

In summary, A pyrene-pyridine hybrid (Py-Py) was used as an axial ligand to bridge Co(II)tetraphenylporphyrin which was finally immobilized on carbon nanotubes via noncovalent interactions and further deposited on glassy carbon. This noncovalent immobilization of Co(II)porphyrin through axial coordination provides significantly enhanced electrochemically catalysed oxygen reductions and oxygen evolutions. As a result, our material (**1/MWCNT/Py-Py**) displayed a catalytic activity far more than the ordinary **1/MWCNT** in all media. The Py-Py moiety served as a direct linker between the cobalt center of the catalyst and MWCNT on electrode. This linker was

DOI: 10.1039/C9NJ02408E

responsible for the enhanced electrocatalytic activities of our material (1/MWCNT/Py-Py). In furtherance, the stability of **1/MWCNT/Py-Py** indicates the strong nature of our system. We can therefore conclude that the strategy of integrating active molecular catalysts in rationally designed Py-Py combined with MWCNT could enable new applications for molecular catalysts in renewable fuel cells.

Conflicts of interest

There are no conflicts to declare.

Acknowledgements

This work was financially supported by the National Natural Science Foundation of China (project 21701058), the Natural Science Foundation of Jiangsu province (project BK20160499), the State Key Laboratory of Coordination Chemistry (projects SKLCC1817), the Key Laboratory of Functional Inorganic Material Chemistry (Heilongjiang University) of Ministry of Education, the China post-doc foundation (No. 2018M642183), the Lanzhou High Talent Innovation and Entrepreneurship Project (No. 2018-RC-105) and the Jiangsu University (project 17JDG035, X. L.).

Notes and references

‡ supporting information is available via xxx

1 Z. Shi, K. Nie, Z.-J. Shao, B. Gao, H. Lin, H. Zhang, B. Liu, Y. Wang, Y. Zhang and X. Sun, *Energy & Environmental Science*, 2017, **10**, 1262–1271.

2 Y. Wu, M. Chen, Y. Han, H. Luo, X. Su, M.-T. Zhang, X. Lin, J. Sun, L. Wang and L. Deng, *Angewandte Chemie International Edition*, 2015, **54**, 4870–4875.

3 W. Zhang, W. Lai and R. Cao, *Chemical reviews*, 2016, **117**, 3717–3797.

4 Y. Lee, J. Suntivich, K. J. May, E. E. Perry and Y. Shao-Horn, *The journal of physical chemistry letters*, 2012, **3**, 399–404.

5 B. Su, I. Hatay, A. Trojánek, Z. Samec, T. Khoury, C. P. Gros, J.-M. Barbe, A. Daina, P.-A. Carrupt and H. H. Girault, *Journal of the American Chemical Society*, 2010, **132**, 2655–2662.

6 G. He, M. Qiao, W. Li, Y. Lu, T. Zhao, R. Zou, B. Li, J. A. Darr, J. Hu and M. Titirici, *Advanced Science*, 2017, **4**, 1600214.

7 F. Cheng and J. Chen, *Chemical Society Reviews*, 2012, **41**, 2172–2192.

8 K. Rabaey and W. Verstraete, *TRENDS in Biotechnology*, 2005, **23**, 291–298.

9 M. Zhou, M. Chi, J. Luo, H. He and T. Jin, *Journal of Power Sources*, 2011, **196**, 4427–4435.

10 W. G. Hardin, D. A. Slanac, X. Wang, S. Dai, K. P. Johnston and K. J. Stevenson, *The journal of physical chemistry letters*, 2013, **4**, 1254–1259.

11 K. Xu, P. Chen, X. Li, Y. Tong, H. Ding, X. Wu, W. Chu, Z. Peng, C. Wu and Y. Xie, *Journal of the American Chemical Society*, 2015, **137**, 4119–4125.

12 J. R. McKone, S. C. Marinescu, B. S. Brunschwig, J. R. Winkler and H. B. Gray, *Chemical Science*, 2014, **5**, 865–878.

13 S. Mukerjee and S. Srinivasan, *Journal of Electroanalytical Chemistry*, 1993, **357**, 201–224.

14 M. Li, L. Zhang, Q. Xu, J. Niu and Z. Xia, *Journal of Catalysis*, 2014, **314**, 66–72.

15 P. K. Sonkar, K. Prakash, M. Yadav, V. Ganesan, M. Sankar, R. Gupta and D. K. Yadav, *Journal of Materials Chemistry A*, 2017, **5**, 6263–6276.

16 P. Du and R. Eisenberg, *Energy & Environmental Science*, 2012, **5**, 6012–6021.

17 B. Reuillard, J. Warnan, J. J. Leung, D. W. Wakerley and E. Reisner, *Angewandte Chemie International Edition*, 2016, **55**, 3952–3957.

18 J. R. Galán-Mascarós, *ChemElectroChem*, 2015, **2**, 37–50.

19 W. Xia, A. Mahmood, Z. Liang, R. Zou and S. Guo, *Angewandte Chemie International Edition*, 2016, **55**, 2650–2676.

20 G. Wu, A. Santandreu, W. Kellogg, S. Gupta, O. Ogoke, H. Zhang, H.-L. Wang and L. Dai, *Nano Energy*, 2016, **29**, 83–110.

21 Q. Lin, X. Bu, A. Kong, C. Mao, X. Zhao, F. Bu and P. Feng, *Journal of the American Chemical Society*, 2015, **137**, 2235–2238.

22 A. Okunola, B. Kowalewska, M. Bron, P. J. Kulesza and W. Schuhmann, *Electrochimica Acta*, 2009, **54**, 1954–1960.

23 K. Kasahara, H. Tsuboi, M. Koyama, A. Endou, M. Kubo, C. A. Del Carpio and A. Miyamoto, *Electrochemical and solid-state letters*, 2006, **9**, A490–A493.

24 W. Zhang, A. U. Shaikh, E. Y. Tsui and T. M. Swager, *Chemistry of Materials*, 2009, **21**, 3234–3241.

25 W. Ma, P. Yu, T. Ohsaka and L. Mao, *Electrochemistry Communications*, 2015, **52**, 53–57.

26 A. Maurin and M. Robert, *Journal of the American Chemical Society*, 2016, **138**, 2492–2495.

27 P. D. Tran, A. Le Goff, J. Heidkamp, B. Jousselme, N. Guillet, S. Palacin, H. Dau, M. Fontecave and V. Artero, *Angewandte Chemie*, 2011, **123**, 1407–1410.

28 A. I. A. El-Mageed and T. Ogawa, *Applied Surface Science*, 2018, **462**, 904–912.

29 Y. Zhou, Y. Shi, F.-B. Wang and X.-H. Xia, *Analytical chemistry*, 2019, **91**, 2759–2767.

30 F. Li, B. Zhang, X. Li, Y. Jiang, L. Chen, Y. Li and L. Sun, *Angewandte Chemie International Edition*, 2011, **50**, 12276–12279.

31 X. Li, H. Lei, X. Guo, X. Zhao, S. Ding, X. Gao, W. Zhang and R. Cao, *ChemSusChem*, 2017, **10**, 4632–4641.

32 A. Rana, B. Mondal, P. Sen, S. Dey and A. Dey, *Inorganic chemistry*, 2017, **56**, 1783–1793.

33 T.-M. Wu and Y.-W. Lin, *Polymer*, 2006, **47**, 3576–3582.

34 T. Zhao, C. Hou, H. Zhang, R. Zhu, S. She, J. Wang, T. Li, Z. Liu and B. Wei, *Scientific reports*, 2014, **4**, 5619.

35 J. Zhu, K. Kailasam, A. Fischer and A. Thomas, *Acs Catalysis*, 2011, **1**, 342–347.

36 Z. Wu, L. Chen, J. Liu, K. Parvez, H. Liang, J. Shu, H. Sachdev, R. Graf, X. Feng and K. Müllen, *Advanced materials*, 2014, **26**, 1450–1455.

37 Z. Sun, J. Li, H. Zheng, X. Liu, S. Ye and P. Du, *International Journal of Hydrogen Energy*, 2015, **40**, 6538–6545.

38 L. Ye, Y. Fang, Z. Ou, L. Wang, S. Xue, Y. Lu and K. M. Kadish, *Journal of Porphyrins and Phthalocyanines*, 2019, **23**, 196–205.

39 F. D'Souza, Y.-Y. Hsieh and G. R. Deviprasad, *Inorganic chemistry*, 1996, **35**, 5747–5749.

40 G. F. Manbeck and E. Fujita, *Journal of Porphyrins and Phthalocyanines*, 2015, **19**, 45–64.

View Article Online
DOI: 10.1039/C9NJ02408E

41 M. A. Ehudin, L. B. Gee, S. Sabuncu, A. Braun, P. Moënne-Loccoz, B. Hedman, K. O. Hodgson, E. I. Solomon and K. D. Karlin, *Journal of the American Chemical Society*, 2019, **141**, 5942–5960.
42 F. D'Souza, G. R. Deviprasad, M. E. Zandler, V. T. Hoang, A. Klykov, M. VanStipdonk, A. Perera, M. E. El-Khouly, M. Fujitsuka and O. Ito, *The Journal of Physical Chemistry A*, 2002, **106**, 3243–3252.
43 J. Cao, D.-C. Hu, J.-C. Liu, R.-Z. Li and N.-Z. Jin, *Journal of Coordination Chemistry*, 2013, **66**, 4211–4219.
44 H. Oshio, T. Ama, T. Watanabe, J. Kincaid and K. Nakamoto, *Spectrochimica Acta Part A: Molecular Spectroscopy*, 1984, **40**, 863–870.
45 L. Boucher and J. Katz, *Journal of the American Chemical Society*, 1967, **89**, 1340–1345.
46 A. Salker and S. Gokakakar, *Int. J of Phys Sci*, 2009, **4**, 377–3844.
47 D. R. Roy, E. V. Shah and S. M. Roy, *Spectrochimica Acta Part A: Molecular and Biomolecular Spectroscopy*, 2018, **190**, 121–128.
48 Z. Xu, H. Li, G. Cao, Q. Zhang, K. Li and X. Zhao, *Journal of Molecular Catalysis A: Chemical*, 2011, **335**, 89–96.
49 A. J. Bard, L. R. Faulkner, J. Leddy and C. G. Zoski, *Electrochemical methods: fundamentals and applications, Wiley New York, 1980.*, Wiley, New York, Wiley.
50 D. Wang and J. T. Groves, *Proceedings of the National Academy of Sciences*, 2013, **110**, 15579.